Acta Scientiarum
http://periodicos.uem.br/ojs
ISSN on-line: 1807-8664
Doi: 10.4025/actascitechnol.v46i1.65754

A modeling strategy for the simulation of box sections with layered shell elements

Jorge Luis Palomino Tamayo[1*], Marcela Palhares Miranda[2] and Inácio Benvegnu Morsch[1]

[1]Programa de Pós-Graduação em Engenharia Civil, Universidade Federal do Rio Grande do Sul, Av. Osvaldo Aranha, 99, 3º andar, Porto Alegre, Rio Grande do Sul, Brazil. [2]Departamento Estrutural, Engecorps Engenharia S.A., Barueri, São Paulo, Brazil. *Author for correspondence: E-mail: jorge.tamayo@ufrgs.br

ABSTRACT. This paper presents a numerical strategy to model box sections from bridge girders using horizontal layered shell finite elements. The basic idea is to avoid the construction of more computational expensive meshes based on the use of folded shell and brick finite elements. The numerical strategy imposes the deactivation of those layers related to empty spaces within the bridge cross-section. The performance of this technique is explored by means of two demanding practical applications related to bridge structures with constant and variable deck thicknesses. The first application deals with the static truck load test of the Caynarachi Bridge, located in Peru, and for which measured field data exists, while the second application is related to the construction stage analysis of a box bridge structure including time effects due to concrete creep, shrinkage and steel relaxation. The results demonstrate that the studied technique acceptably correlates with the measured field data,expressed in terms of vertical displacements,with correlation coefficients exceeding 0.94.Additionally, the outcomes align well with the results of other numerical techniques, allowing applicants to use this simplified modeling approach in daily design office.

Keywords:girders; concrete structures; finite-element modeling.

Received on November 9, 2022.
Accepted on July 21 2023.

Introduction

The numerical modeling of bridges using the Finite Element Method (FEM) is a customary task in design offices and research institutes at universities, in which efficient modeling techniques are searched. The simulation of constructional loads is an important phase of the structural analysis as time effects might have a significant outcome during the construction process of the structure. Hence, a reliable numerical model should be able to trace the desired bridge profile as required in the project. On the one hand, the elaboration of numerical models using brick and folded shell finite elements are advantageous, since the actual deformational behavior can be well captured at both the local and global level. However, millions of degrees of freedoms may be needed for elaborating such models, being more helpful for a preliminary stage of analysis the use a simplified modeling technique. On the other hand, the use of spatial one-dimensional beams elements substantially reduces the number of unknowns, but the actual biaxial stress state, shear lag effect and cracking patterns in a Reinforced Concrete (RC) deck cannot be realistically well captured. Therefore, an efficient modeling technique searches for a compromise between numerical accuracy and a reasonable representation of the structural behavior. Then, this work applies a simplified modeling technique, based on the use of horizontal layered shell finite elements, for modeling complex hollow box sections or concrete decks with variable thicknesses. It seems that this approach has not receivedso much attention from practitioners according to the revision made in Miranda, Tamayo, and Morsch (2022), maybe due to the lack of application of this technique in the numerical modeling of challenger examples, so this paper aims to fulfill this gap.

Papers related to the numerical modeling of bridge structures using brick elements, folded shell elements, planar and spatial beam elements are commonly found in the technical literature. To cite a few, Shushkewich (1986) used a two-node planar one-dimensional beam element to model the time-dependent analysis of segmental bridges. Ates (2011) established a 3D Finite Element (FE) model using the software SAP 2000 (2008) for the long-term analysis of the Budan Bridge located in Turkey. Shell and beam-column elements were used to model the deck and pier, respectively. In Nimse, Nims, Hunt, and Helmicki(2015), a 3D FE model using spatial beam elements from LARSA (2021) software was employed to model a cable-stayed bridge located in Toledo, Ohio.

In Vookunnaya, Ravindranatha, and Thite(2017), a pre-stressed three-span continuous concrete box girder bridge with varying cross sections was studied using the MIDAS (2017) software. In Su, Nassif, and Xia(2018), a typical three-span continuous bridge was analyzed with a nonlinear 3D FE model built in ABAQUS (2012) software. The model was comprised of shell elements for modeling the concrete slab, and two-node beam elements to model the steel girder and box beams. In Butler et al. (2018), the sequential process of a composite bridge was analyzed using a three-dimensional model in DIANA (2015) software,using brick elements to model both the concrete deck and steel beam. In Wang, Zhu, Zhou, Han, and Ji(2020), composite continuous girder bridges were assessed during constructional loads using a FE model in ANSYS (2007). Their model used shell finite elements for modeling the concrete slab and steel beam. In Han, Zhang, Zhou, and Lan(2020), an analytical approach was presented to compute secondary internal forces generated due to concrete creep in steel-concrete composite beams, using theANSYS (2007) softwareand brick elements with linear elastic behavior.

In He et al. (2020),a steel-concrete composite box girder was studiedusing a FE model in MIDAS (2017) software. The model was comprised of spatial beam elements to describe variable cross sections, including long-term effects. In Wang, Wang, Sun, Mao, and Tang (2020), a direct and fast method to avoid cumulate calculations from past loading history applied to self-anchored suspension bridges was proposed. Any bridge structure is spatially modeled by means of 3D beam elements and catenary-cable elements.In Li, Huang and Guo (2021), the vulnerabilities of bridges under construction loads due to the action of strong earthquakes were evaluated. A case study bridge was analyzed using a finite element model built in MIDAS (2017) software together with the cast-in-place cantilever construction method. The cushion caps and girders were all modeled with beam elements. Motlagh and Rahai (2021) studied the long-term performance of a prestressed concrete bridge with corrugated steel webs built in Iran. The bridge was modeled in ABAQUS (2012) software by using ten-node tetrahedral solid elements for representing the concrete members and external tendons, while two-node truss and shell four-node elements were used for representing the internal cables and corrugated steel webs, respectively.

In Zhu, Wang, Zhou, and Han (2022), the structural health monitoring of an I-shaped steel-concrete composite girder bridge during construction was assessed. The FE model was built in ANSYS (2007) software, using shell elements to simulate the steel beams, concrete slabs, and permanent steel formwork, while beam elements were employed to simulate the studs and the lateral bracing system. Wang, Thrall, Zoli, and Sun (2022) introduced a technique to measure the behavior of long-span bridges during intermediate stages. To validate this technique, a local 3D finite element model of an end floor beam built in ABAQUS (2012) was used to verify the measured strains between two intermediate stages. In Huang, Ke, and Hu (2023), a comprehensive study of the Xiangsizhou Bridge built in China was performed. This is a double-tower double-cable-steel-concrete composite girder cable-stayed bridge. The proposed finite element model was built in MIDAS (2017) commercial software.The steel-concrete composite beam was simulated using a double main beam, with the steel main beam and the bridge deck modeled separately as beam elements.

From the aforementioned works, the regular modeling technique implies the use of brick elements, folded shell elements, beam elements or a combination of them for the stage constructional analysis of bridges. Conversely, this paper aims to evaluate the performance of a simplified modeling technique based on the use of horizontal layered shell finite elements to represent box girder bridges under flexural loads. Basically, the procedure involves the partial or total deactivation of those particular layers related to empty zones within the girder cross-section. By showing the robustness of this modeling strategy, stakeholders may count on with another alternative to elaborate their numerical models. For such scope, an institutional computer program developed by the authorsand which has been subject of various research works (see e.g.,Miranda et al., 2022 andDias, Tamayo, Morsch, &Awruch, 2015) is modified accordingly.

Material and methods

The long-term concrete constitutive model and finite element available in the developed finite element tool, alongside the studied cases are briefly described in the following sections.

Long-term constitutive model for reinforced concrete

The integral of Volterra, as written in Eq.1, defines the stress-strain relationship of linear viscoelasticity using the Boltzmann's superposition principle. This equation is a general uniaxial representation of an aging viscoelastic material.

$$\varepsilon(t) = \int_0^t J(t,t')\, d\sigma(t') + \varepsilon_0(t) = \varepsilon_c(t) + \varepsilon_{sh}(t) \quad (1)$$

where $J(t,t')$ is the creep compliance function representing the total deformation at time t for a unit stress applied at time t', $d\sigma(t')$ represents a small increment of stress applied at t', $\varepsilon_{sh}(t)$ is the nonmechanical strain due to shrinkage and $\varepsilon_c(t)$ is the mechanical strain involving the instantaneous elastic $\varepsilon_{ci}(t)$ and concrete creep $\varepsilon_{cc}(t)$ strains. Upon temporal integration of this expression at two consecutive time instants t_i and t_{i-1} with a linear approximation for stresses, the creep incremental strain within a general time interval $\Delta t_i = t_i - t_{i-1}$ can be expressed in a recursive manner as follows:

$$\Delta\varepsilon_{cc}(t_i) = \sum_{\mu=1}^{N} \varepsilon_\mu^*(t_{i-1})\left[1 - e^{-\Delta t_i/\tau_\mu}\right] + \sum_{\mu=1}^{N} \frac{1}{E_\mu(t_{i-\zeta})}\left[1 - \frac{\tau_\mu}{\Delta t_i}\left(1 - e^{-\Delta t_i/\tau_\mu}\right)\right]\Delta\sigma(t_i) \quad (2)$$

with,

$$\varepsilon_\mu^*(t_{i-1}) = \varepsilon_\mu^*(t_{i-2})e^{-\Delta t_{i-1}/\tau_\mu} + \frac{\tau_\mu}{\Delta t_{i-1}}\left(1 - e^{-\Delta t_{i-1}/\tau_\mu}\right)\frac{\Delta\sigma(t_{i-1})}{E_\mu(t_{i-1-\zeta})} \quad (3)$$

in which $E_\mu(t')$ and τ_μ are the age-dependent modulus and retardation time of the μ-th term of a Dirichlet series with N terms used to approximate the creep function $C(t,t') = J(t,t') - 1/E_c(t')$, respectively, while $\zeta = 1/2$ refers to the middle of the current time interval. Thus, the incremental quasi-elastic stress-strain relationship, after some manipulation and suitable for numerical implementation, can be expressed in the following manner (Dias et al., 2015).

$$\Delta\sigma(t_i) = \sigma(t_i) - \sigma(t_{i-1}) = E^*(\Delta\varepsilon - \Delta\varepsilon_0) \quad (4)$$

where parameters E^* and $\Delta\varepsilon_0$ are uniaxial quantities referring to an equivalent material modulus and incremental initial strain due to creep and shrinkage strains, respectively, and whose three-dimensional generalization can be easily obtained (Dias et al.,2015). In this manner, the rheological problem can be treated as a quasi-elastic analysis with nonzero initial strains $\Delta\varepsilon_0$. In the particular case of the stress-strain relationship of pre-stressed tendons, a stress term $\Delta\sigma_{p,T}$, referring to the initial stress installed in the tendon at the beginning of the analysis, should be added to the right-hand side of Eq. (4).

In the case of staged constructional analysis, the current algorithm follows the Ghost Approach (SAP2000,2008,Miranda et al.,2022), in which the FE mesh of the whole structure is modeled since the beginning of the analysis. Initially, all elements are attributed a very small stiffness value according to the numerical precision of the computer. Then, activated elements assume their actual stiffness values from the stage in which they firstly appear.

Layered finite element

The RC finite element is originally represented by a curved thick layered shell element with eight nodes at its middle-plane and five degrees of freedom at each node, three translations and two in-plane rotations as shown Figure 1(a). Several layers through the shell thickness referred to the middle-plane surface are then defined in order to capture material nonlinear behavior within the element as shown in Figure 1(b) (Haido, Abu Bakar, & Abdul-Razzak, 2010). Commonly, eight to twelve layers are employed to yield accurate results. The element is able to simulate the variability of the thickness within the element across its middle surface as the top and bottom coordinates may be defined at each node (Tamayo, Morsch, &Awruch, 2013). This special feature distinguishes this element from the common flat ones, allowing therefore the modeling of curved surfaces as may be encountered in RC decks. However, the modeling of explicitly folded plate structures is not allowed in the original formulation of the element. This is because the nodal coordinate system at each node is used for all elements that share this node, not allowing therefore the nodal decoupling among these elements.

In this paper, a particularization of the current curved element to the situation of a flat one depicted in Figure 1(c) is accomplished by using a constant thickness through the element. Indeed, the nodal coordinate system defined at each node may coincide with the Cartesian global coordinate system in the case of horizontal shell elements, as shown for node 5. In this context, the only data that must be provided are nodal coordinates of the middle plane and element thickness.

In relation to internal pre-stressed tendons or discrete reinforcing bars, they can be represented within the element by employing embedded one-dimensional curved elements with three nodes as displayed in Figure 1(a), whereas steel reinforcing meshes can be defined at their corresponding locations by equivalent membrane layers.

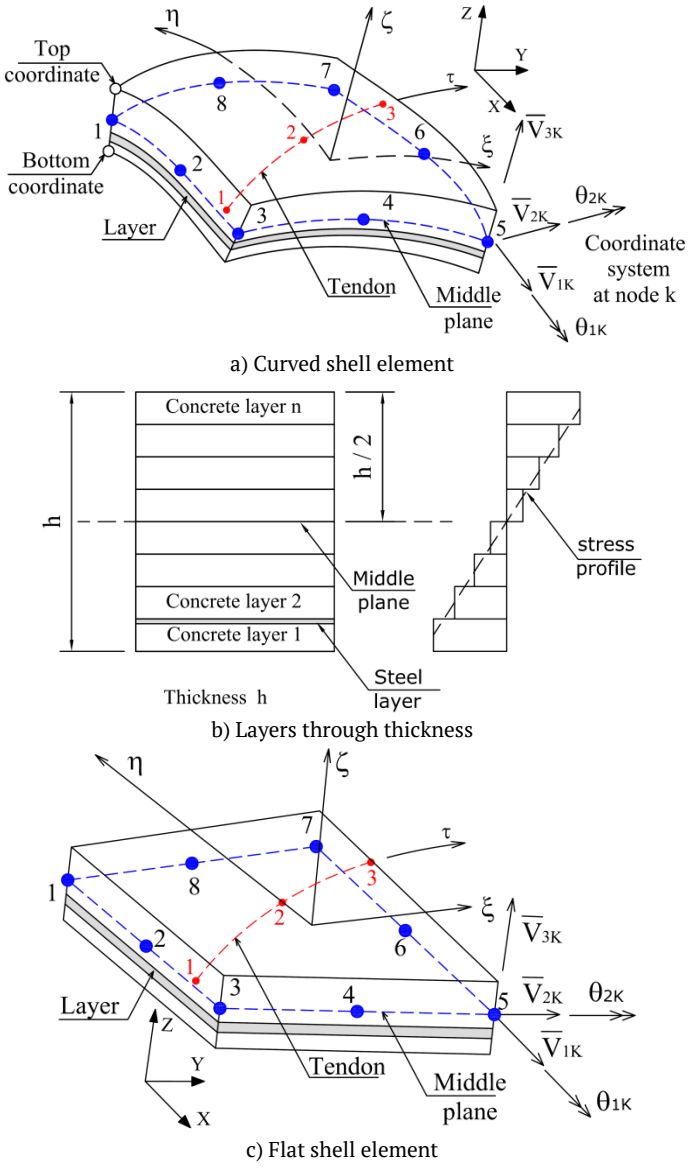

a) Curved shell element

b) Layers through thickness

c) Flat shell element

Figure 1. Layered finite elements.

Numerical strategy for modeling box sections

The schematic representation of the regular modeling of box or hollow cross-sections using brick and shell finite elements are depicted in Figure 2(a) and Figure 2(b), respectively, where it can be observed that the walls are explicitly modeled with vertical elements in these meshes. Nevertheless, the box cross-section can be also modeled by deactivating the corresponding concrete layers through the cross-section depth, as displayed in Figure 2(c), using layered shell elements.

The deactivation process is accomplished within the FE code by the creation of an input parameter β, which ranges from zero to one, and which directly multiplies the volume associated to any specific layer. Thus, as the layer volume affects the computation of the element stiffness matrix and internal force vector, the β parameter has a direct impact on the evaluation of these quantities. In this manner, a significant modification of the programming style within an existing FE code is avoided. This modeling strategy can be also used with some commercial software, as they usually provide a "modification stiffness factor" option in the element definition.

A value of $\beta = 0$ implies that the volume associated to that specific layer (inactive layer) is null, eliminating therefore any contribution of the layer to the stiffness and strength of the element it belongs to.Conversely, a value of $\beta = 1$ will indicate a full contribution of the current layer (active layer) as occurred in the usual case, whilst an intermediate value will implicate a partial contribution. In this

manner, if adjacent layers across the depth of the section are defined with different β values, the desired profile of the cross-section can be traced. In addition to this, the cross-sectional division must accompany the adopted discretization of the FE mesh in plant. For instance, the thickness of the wall elements depicted in Figure 2(c) will dictate the discretization of the FE mesh in plant as shown in Figure 2(d). This is because these vertical elements are associated to fully activate layers, unlike the central part and overhangs of the cross-section, where inactive layers are necessary.

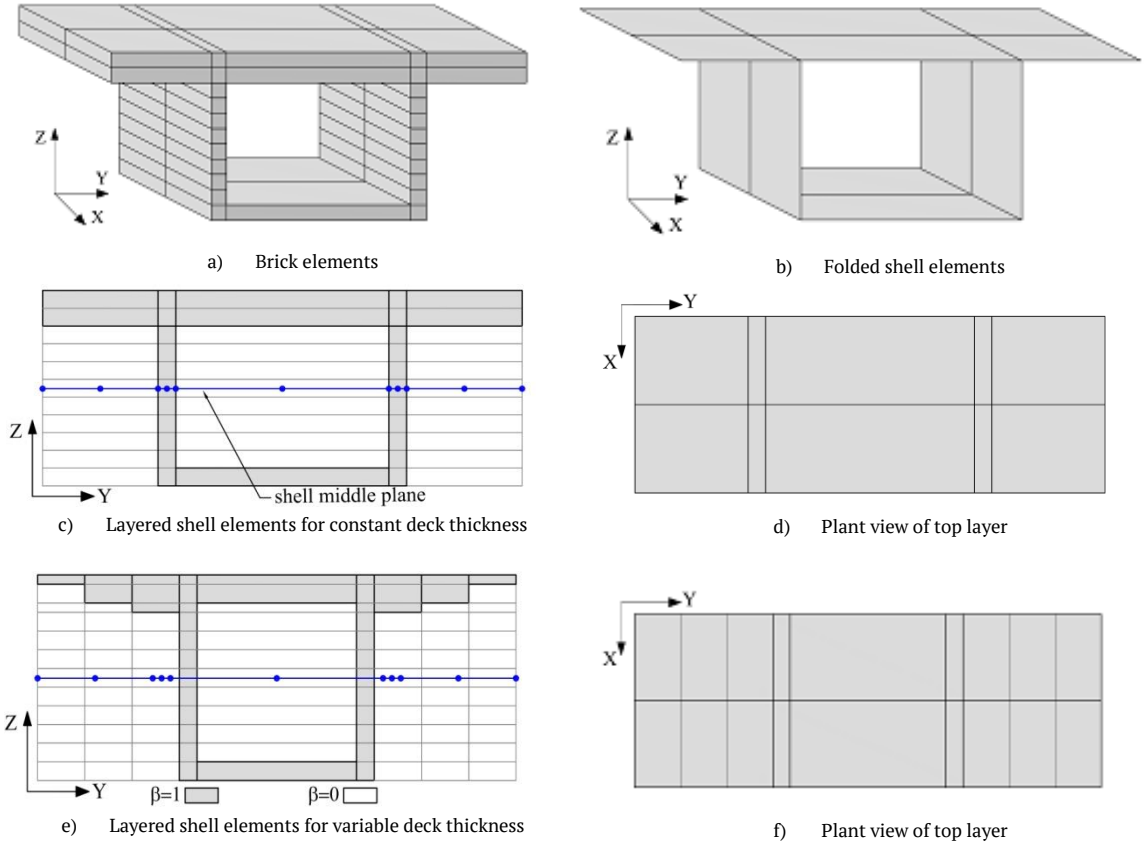

a) Brick elements

b) Folded shell elements

c) Layered shell elements for constant deck thickness

d) Plant view of top layer

e) Layered shell elements for variable deck thickness

f) Plant view of top layer

Figure 2. Schematic representation of modeling techniques for representing box sections with finite elements.

A more complicated situation arises when the concrete deck has a variable thickness across its width, as occurred in some real girder cross-sections. In such situation, the original degenerated shell element with variable thickness may be invoked, but its availability may be restricted in some commercial software. Another alternative is to use a series of flat layered shell elements of different constant thicknesses across the section width alongside deactivated layers, so that the thickness variation of the deck can be traced as shown in Figure 2(e). In fact, this latter approach will be preferred in this paper for studying the practical examples from the next section.

Clamped beam loaded at its free end

The proposed numerical strategy is applied here to the numerical modeling of the clamped beam illustrated in Figure 3(a) subjected to a load P at its free end, regarding a linear elastic behavior of the material with an elasticity modulus of E=30 GPa and Poisson's ratio of zero. A null Poisson's ratio means that there is no coupling between the stress and strain in mutually orthogonal directions.Two cross-sections are deemed in the analyses: the first case (Case 1) depicted in Figure 3(b) considers a simple rectangular box section with deck and wall constant thicknesses, while the second case (Case 2) deals with a complex trapezoidal cross-section with variable thickness for the overhangs, where, due to symmetry considerations, only half of the cross-section is sketched in Figures 3(c)-(e). For the second case, the use of the original curved shell element from Figure 1(a) is employed to model the variable thickness of the cross-section. Here, three subcases named case 2a, case 2b and case 2c related to the cross sections displayed in Figure 3(c), Figure 3(d) and Figure 3(e), respectively, are considered. The basic idea for cases 2a and 2b is to show the numerical modeling of the same

filled trapezoidal cross-section in two different manners, while case 2c depicted in Figure 3(e) is similar to previous ones, but with a rectangular hole at its center. The layout of the FE mesh in plant at all cases accompanies the adopted discretization of the cross-section width with 12 divisions along this direction (direction Y) and 15 divisions along the longitudinal direction of the beam (direction X), employing therefore a total of 180 eight-node layered shell elements. The empty spaces illustrated in Figure 3(d) and Figure 3(e) are modeled assigning zero values for the β coefficient in the corresponding layers.

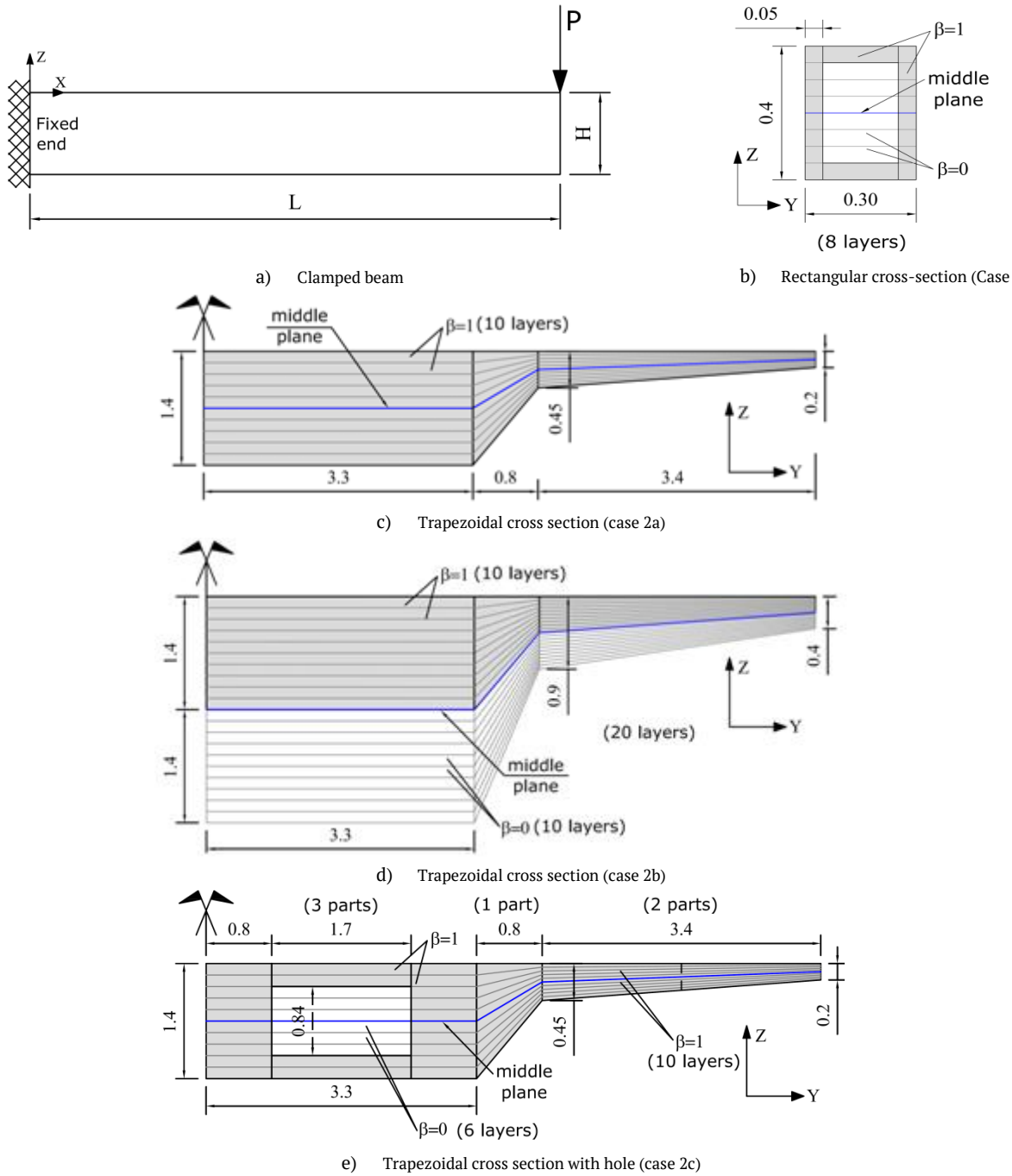

a) Clamped beam

b) Rectangular cross-section (Case 1)

c) Trapezoidal cross section (case 2a)

d) Trapezoidal cross section (case 2b)

e) Trapezoidal cross section with hole (case 2c)

Figure 3. Bridge cross-sections (Units in meters).

Static truck load test of the Caynarachi bridge

The Caynarachi Bridge is a semi-integral three-span continuous bridge constructed in Peru in 2004, and highlighted in the work of Manso, Martinez, Diaz, Fresno, and Rabanal (2015) for its construction method. It has two outer spans of 40 m and a central span of 50 m, its cross section is comprised of a RC deck with variable thickness supported by two steel profiles as shown in Figures 4(a)-(b). The static truck

load test of the bridge was carried out after three months of its construction and consisted in positioning three trucks in series at each span one at a time. When the trucks are positioned at a given span, the corresponding field measurements of vertical displacements along the longitudinal axes 1 and 2 from Figure 4(b) are noted.

a) View of Caynarachi bridge

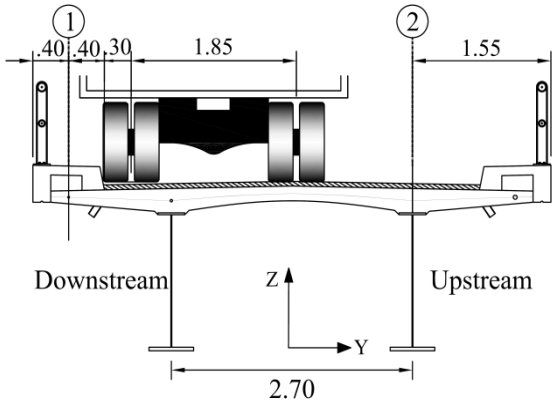

b) Cross section

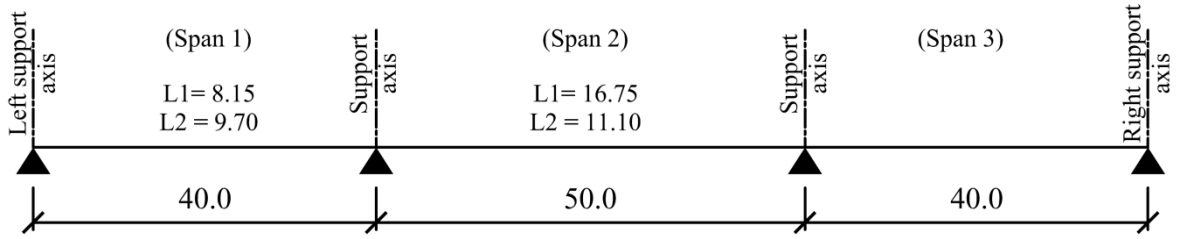

c) Beam profile

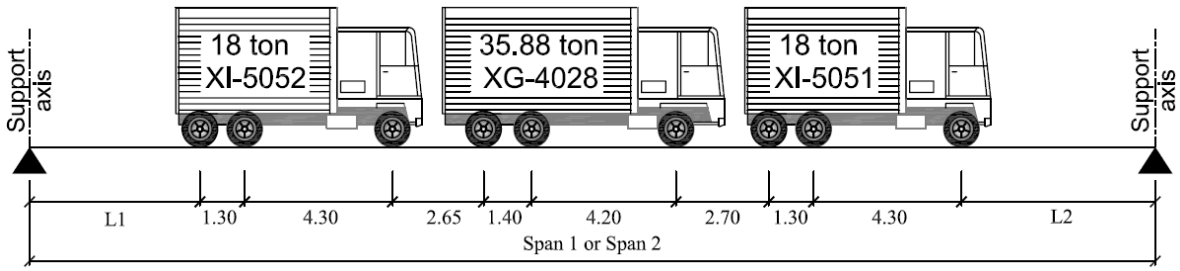

d) Typical loaded span

Figure 4. CaynarachiBridge: truck load test (Units in meters).

The typical position of the trucks for the first or second span is defined in Figure 4(d), whereas the position of the trucks for span 3 is symmetric in relation to the first span. A linear elastic analysis is performed for the complete bridge superstructure with the following properties: elasticity modulus of E_c= 38GPa and Poisson's ratio of 0.2 for concrete, and elasticity modulus of E_s= 200GPa and Poisson's ratio of 0.3 for the steel profile. Special beam-column elements for representing the channel shear connectors are located at discrete locations to model partial interaction (Dias et al., 2015). At the external and interior support zones, connectors are spaced at 30 cm, while they are spaced at 45 cm between supports. The three-dimensional FE mesh used to capture the as built behavior of the bridge is depicted in Figure 5, while the actual and adopted cross-sections are depicted in Figure 6(a) and Figure 6(b), respectively. It is noticed that the actual thickness variation of the concrete deck has been approximated by various flat shell elements in series with different number of active layers across the deck width. Special attention has been given to ensuring that the second moments of area of the actual and equivalent concrete deck are practically the same. The bottom slab and diaphragm beams are also considered in the FE model, as they are defined in the zones near the interior supports and along the steel beam, respectively. Furthermore, the reinforcing bars in the slabs have been considered as additional steel layers of equivalent thickness according to Figure 1(c).

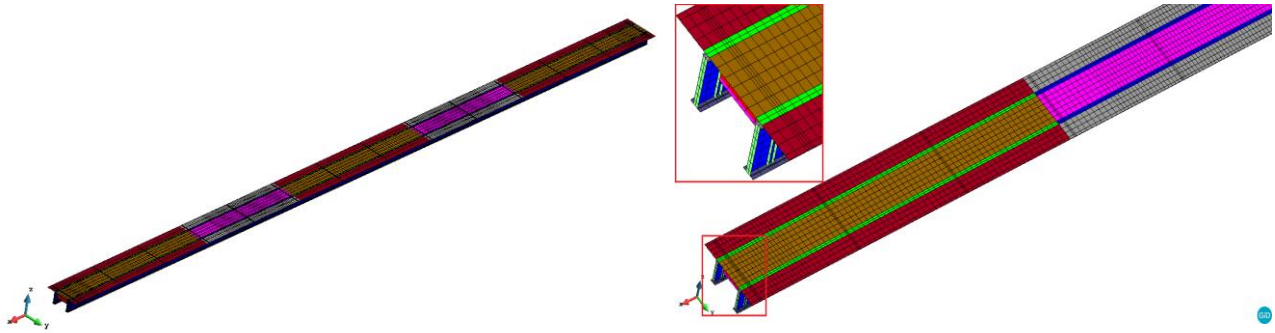

a) 3d view b) Bridge cross-section

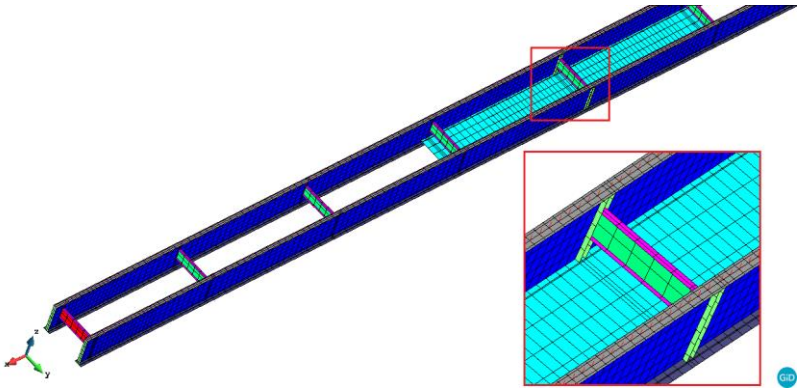

c) Detail of diaphram beams

Figure 5. Details of finite element mesh.

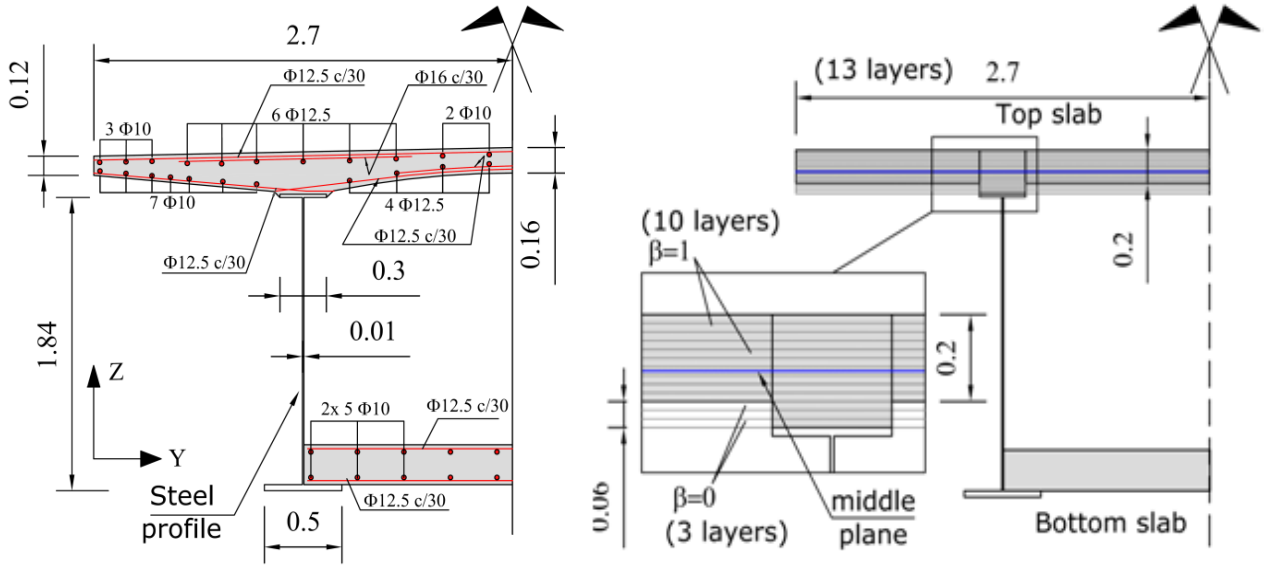

a) Actual cross section b) Equivalent cross section

Figure 6. Caynarachi bridge cross section (Units in meters).

Construction stage analysis of a pre-stressed box bridge

The construction stage analysis of a pre-stressed concrete box girder bridge made up of precast segments is performed in this section. The bridge geometry and tendon profiles are similar to that presented in the works of Tadros, Ghali, and Dilger (1979) and Shushkewich (1986). Unlike these works, a constant cross-section depth and straight tendon profiles are used here as shown in Figure 7. The bridge has three-spans of 53.5m, 65 m and 53.5 m with a total length of 172 m. Its construction schedule is graphically depicted in Figure 8, where each number in the circle refers to the constructive phase in which a member is introduced. Table 1 lists the duration in days of each stage.

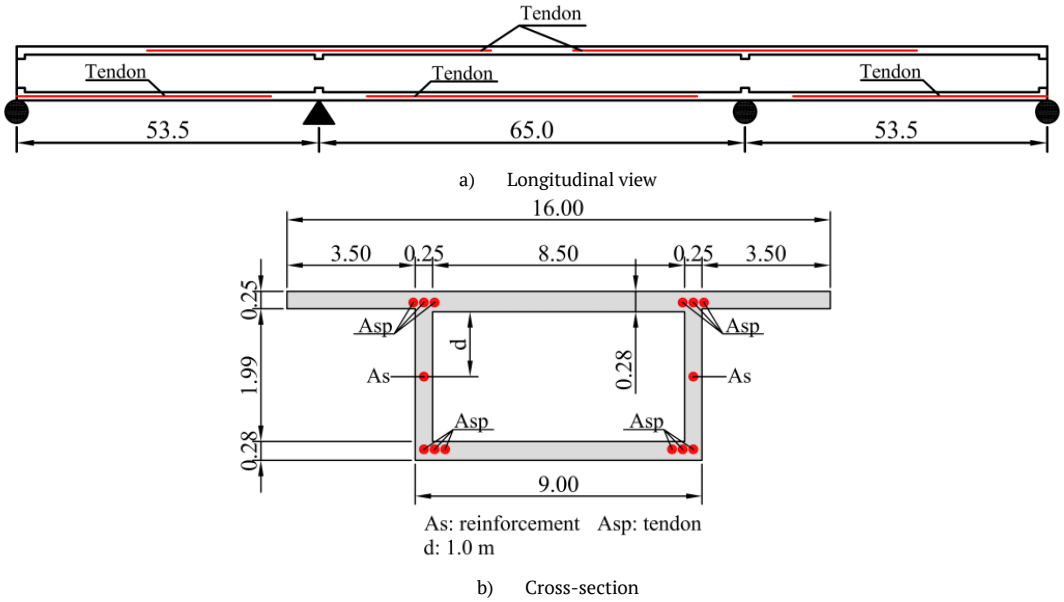

Figure 7. Bridge geometry (Units in meters).

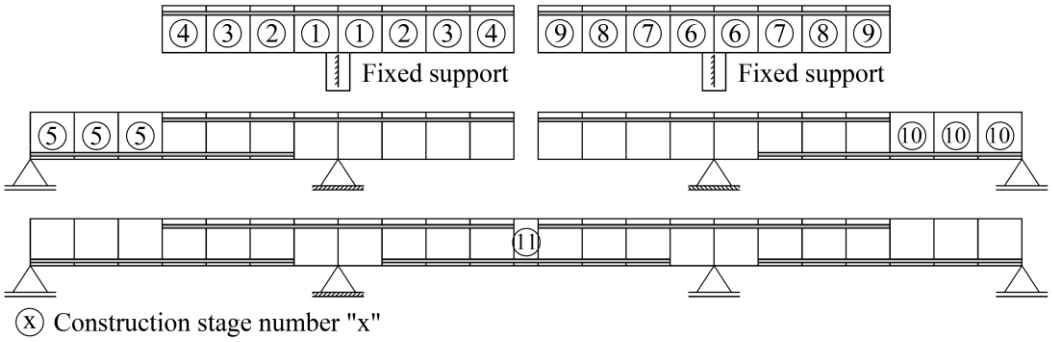

Figure 8. Construction sequence.

The precast segments were cured for 3 days and stored until the beginning of the execution. The applied loads are the self-weight of the structure and the pre-stressed force applied to the low-relaxation steel tendons. The target pre-stressing stress at the end of the installing operation is 1260MPa. The ACI-209 model code (1992) for concrete creep and shrinkage was used for the long-term analysis with cement type III, moisture content of 40%, ultimate creep coefficient of 2.0 and ultimate shrinkage strain value of $300x10^{-6}$. Material properties are listed in Table 2.

Table 1. Details of the construction phases.

Duration (days)*	Stage	Activities
30	1	Stages 1 to 4, cantilever erection. Assembly of the pre-cast segments and activation of pre-stressing for top tendons. Interior support is fixed against rotation and translation.
33	2	
36	3	
39	4	
43	5	Completion of span 1. Assembly of pre-cast segments near the left external support, activation of pre-stressing for bottom tendons, and change of support to hinge support in the interior support.
47	6	Similar to stages 1 to 4, cantilever erection. Assembly of the pre-cast segments at the other interior support and activation of pre-stressing for top tendons. Interior support is fixed against rotation and translation.
50	7	
53	8	
56	9	
60	10	Completion of span 3. Assembly of pre-cast segments near the right external support, activation of pre-stressing for bottom tendons, and change of support to hinge support in the interior support.
63	11	Introduction of continuity in the central span. Assembly of the central segment and activation of the pre-stressing for bottom tendons.

*Considering the age of the concrete.

Table 2. Materials properties.

Material	Properties	
Concrete	Elastic modulus(28 days) (GPa)	35
	Poisson's ratio	0.0
	Compression strength(28 days) (MPa)	54
Reinforcement	Elastic modulus (GPa)	200
	Yield stress (MPa)	585
	Total area (cm^2)	222
Tendon	Elastic modulus (GPa)	190
	Yield stress (MPa)	1500
	Area (sup[1].) (cm^2)	126
	Eccentricity* (sup.[1]) (cm)	120
	Area (inf.[2]) (cm^2)	81.5
	Eccentricity* (inf.[2]) (cm)	125

*Considering the centroid [1]upper tendon [2]bottom tendon.

The FE mesh alongside the adopted cross-section to simulate the box section is depicted in Figure 9. The hollow box section is formed with the use of zero β coefficients for the layers in the overhangs and for those intermediate layers in the central region, with exception of the upper layers, which are associated to the concrete deck.

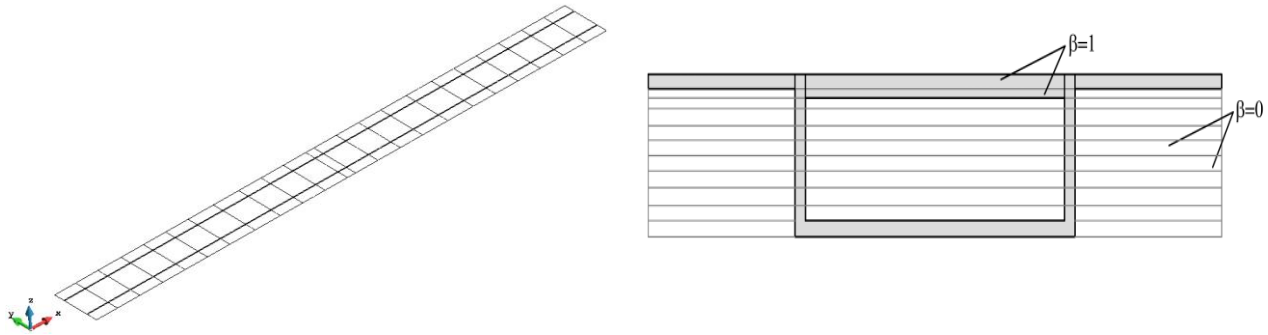

a) Isometric view of the middle plane b) Cross-section

Figure 9. Finite element mesh.

Results and discussion

The outcomes and corresponding discussions of the examples of the preceding section are presented here.

Clamped beam loaded at its free end

The numerical deflection δ_{NUM} and rotation θ_{NUM} at the free end for each case are compared with the analytical solutions δ_{ANA} and θ_{ANA} in Table 3, with $\delta_{ANA} = PL^3/3EI$ and $\theta_{ANA} = PL^2/2EI$, in which L is the beam length and I is the second moment of area of the section.

Table 3. Deflection and rotation at free end.

Case	L/H	I (m^4)	$\delta_{NUM}/\delta_{ANA}$	$\theta_{NUM}/\theta_{ANA}$
1	5.0	1.15E-03	1.046	1.009
2a	40.71	2.2047	1.009	1.009
2b	40.71	2.2047	1.009	1.009
2c	40.71	1.9900	1.008	1.007

From Table 3,it is noticed that the numerical quantities overestimate the analytical ones at all cases. Indeed, the associated error of the numerical deflection is +4.6% for case 1, +0.9% for cases 2a and 2b and +0.8% for case 2c, while the error in the computation of the numerical rotation is +0.9% for cases 1, 2a, 2b and 0.7% for case 2c. It is important to mention that,for the sake of computational simplicity,the analytical formulas used in this study do not account for the small contribution of the shearing deformation. In general, the agreement is quite acceptable from a practical viewpoint. In case 2a (the reference case), none advantage is taken of the proposed technique, and the thickness variation of the cross-section is considered by defining the top and bottom nodal coordinates of the curved shell elements. For case 2b, a fictitious cross-section with a greater depth, e.g., twice the

original depth, is then used. Here, fictitious layers with null β coefficients are assigned to the bottom layers of the section to establish a middle plane that passes at the bottom of the actual cross-section. The idea is to omit those layers below this plane, so that the actual cross-section from case 2a can be recovered. Special care has been taken to ensure that the same number of active layers is employed for cases 2a and 2b, in order to make a proper comparison between them. As the middle-plane in each case is different, the nodal restraints at the clamped ends are also applied to different planes. Although this situation has not brought significant differences in the results listed in Table 3, the reader should be aware of this situation.

Static truck load test of the Caynarachi bridge

Figure 10 illustrates a comparison between the vertical displacements obtained from the FE model along the longitudinal direction of the bridge, corresponding to axes 1 and 2 from Figure 4(b), and the measured field data. The comparison is conducted for various cases in which the trucks are positioned at different spans. It is noted that the numerical prediction is quite acceptableat various longitudinal stations, taken into consideration that the adopted elastic modulus of concrete directly corresponds to that predicted by the ACI-209 model code (1992) for the time at which the truck load test was accomplished. The computed correlation coefficients between the measured and computed vertical displacements are greater than 0.94. The encountered differences may be attributed to the support conditions adopted in the present FE model as perfect hinges. The use of flexible support conditions based on springs may improve the numerical prediction.

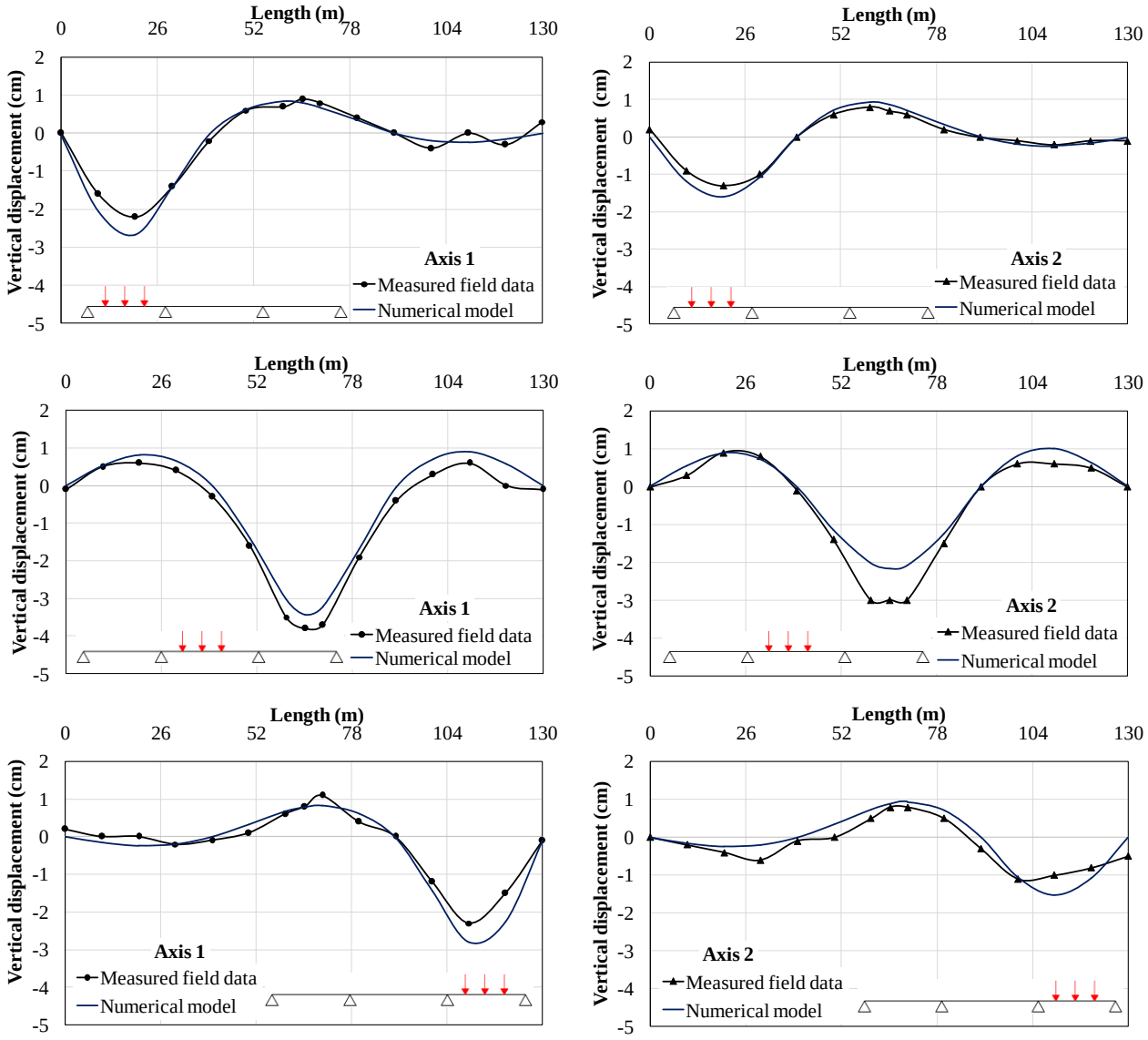

Figure 10. Vertical displacement along beam axis.

The deflection profile along the longitudinal axis of the beam, obtained from the current FE model, is depicted in Figure 11 and compared with the results obtained from the particular computer code made available by Shushkewich (1986) to deal with the construction stage analysis of bridges (named "Beam" in the graphs) using two-node beam elements. As it may be observed, the displacement profiles are very similar between both approaches, indicating therefore that the current technique is able to capture properly the bridge response at the global level. Also, the histories of longitudinal stresses at the top and bottom fiber of the cross-sections, located close to the left interior support and at the middle section of the interior span, are compared in Figure 12 for the complete period of analysis. The stress profiles are quite similar for both approaches, highlighting therefore the adequacy of the present model, also at the local level. Although it is not expected the same identical response, the observed differences are related to the computation of the creep coefficient, temporal discretization, intrinsic nature of each modeling technique and the treatment of material ageing.

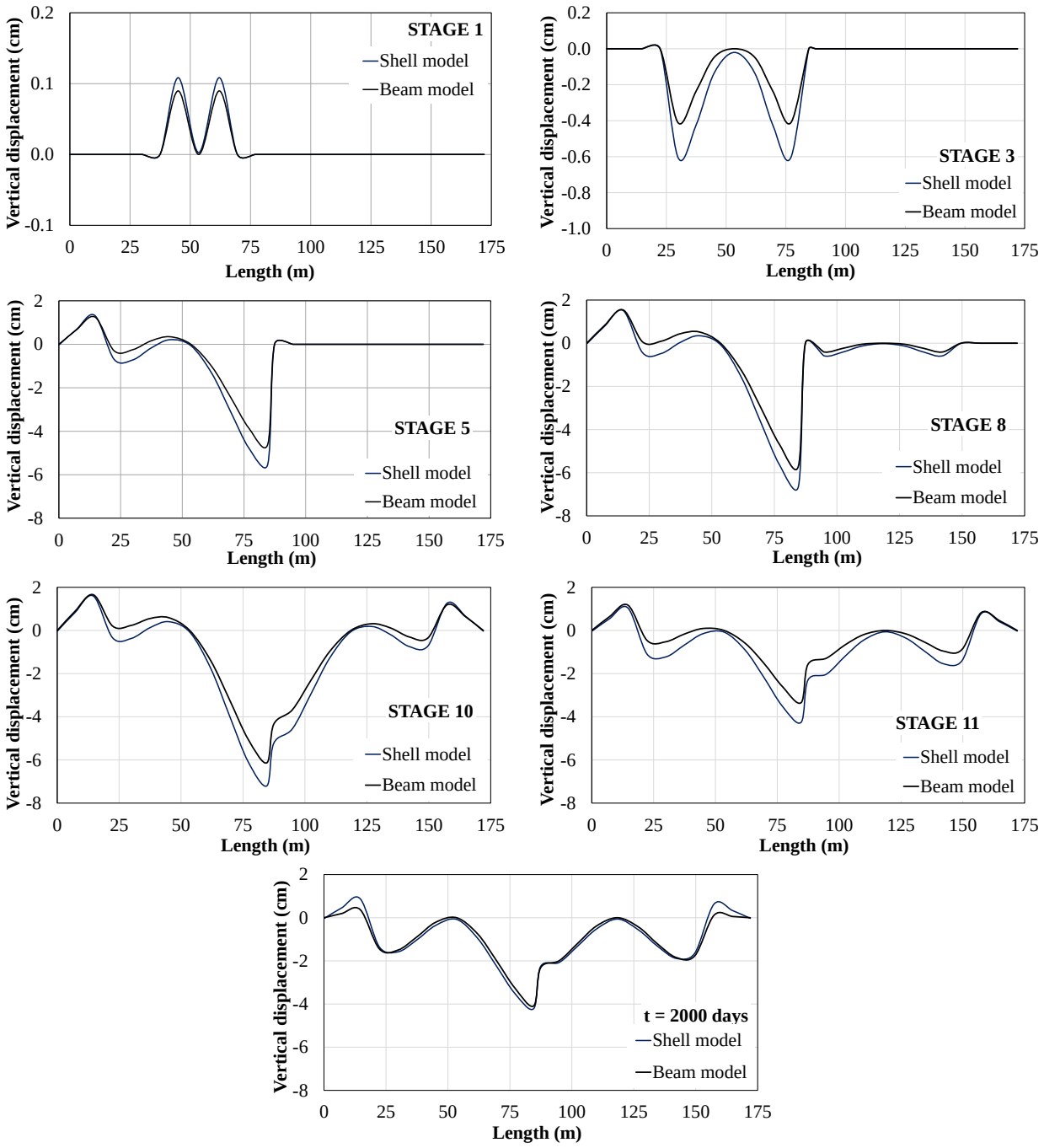

Figure 11. Vertical displacement at different stages.

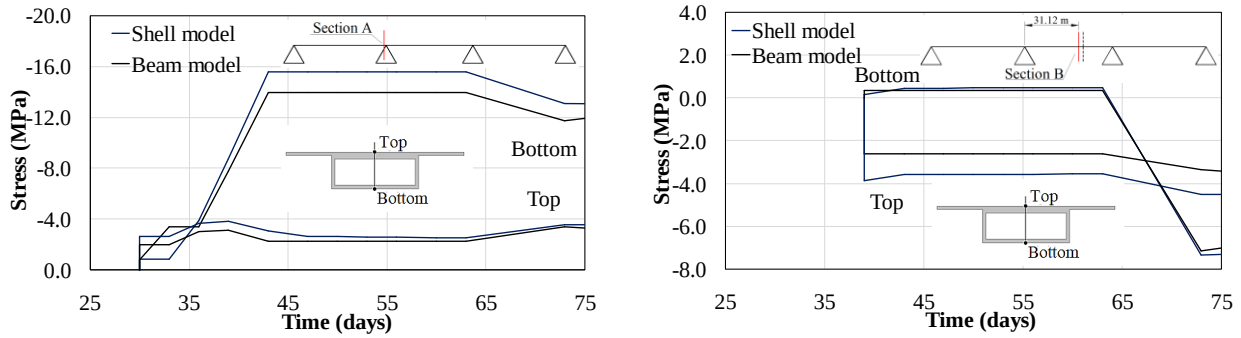

Figure 12. Longitudinal stress variation.

Furthermore, the evolution of the longitudinal stress for the top concrete layer of the deck is depicted in Figure 13 at various stages. It is interesting to note that the longitudinal stress field is not constant across the deck width, as occur in Shushkewich's model based upon beam elements. Thus, the modeling technique presented herein demonstrates its potential for accurately representing the true behavior of the concrete deck in a more consistent manner.

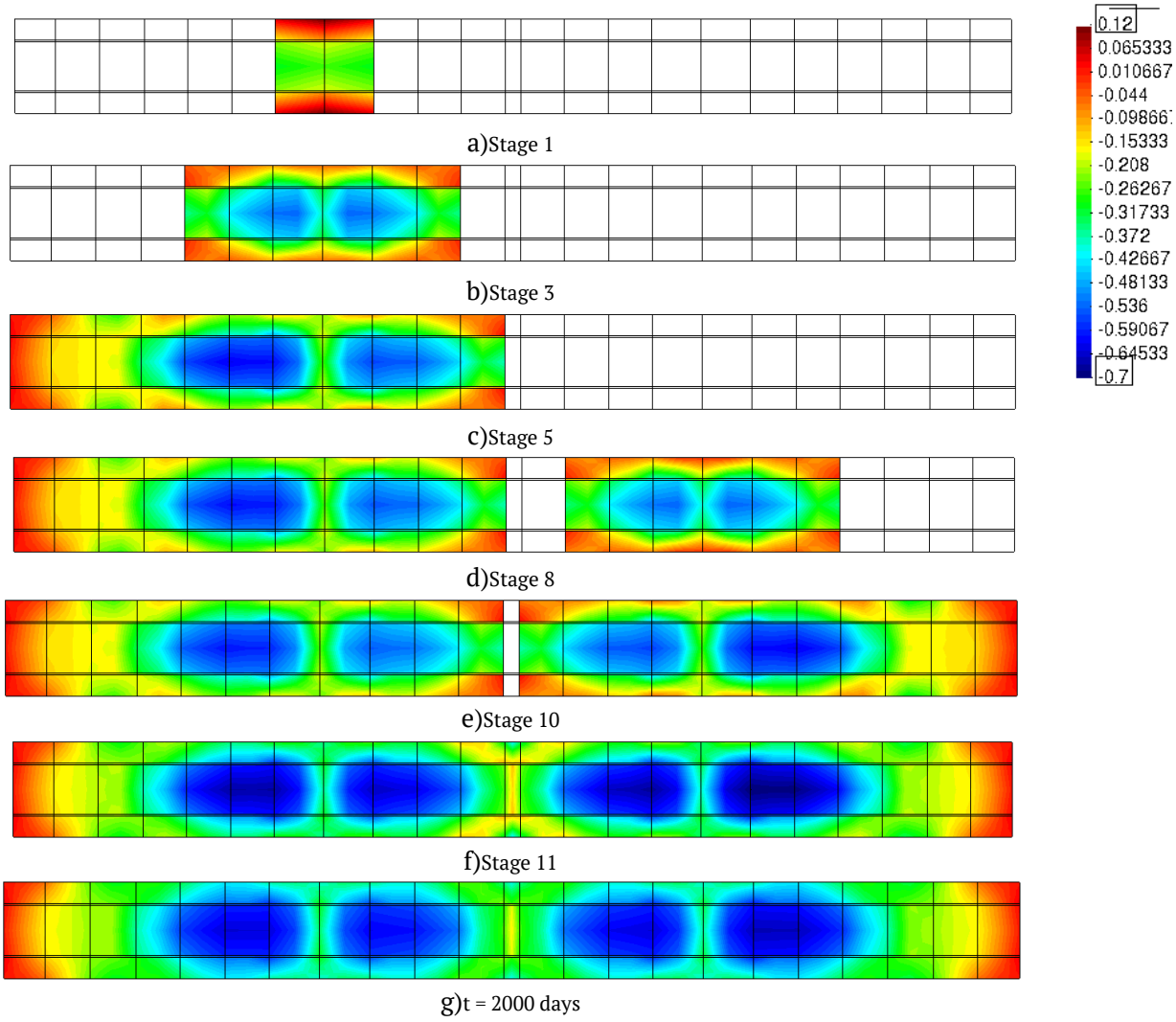

Figure 13. Longitudinal stress (x10 MPa) field evolution with stages for the top layer of the deck.

Conclusion

This paper deals with the modeling strategy of box cross-sections from bridge girders using horizontal layered shell elements, where decks with variable thickness and hollow cross-section can be modeled by deactivating the required specific layers. From this, the following conclusions can be drawn:

The present modeling technique proved to be accurate in computing the deflection at the free end of a clamped beam, when compared with the corresponding analytical solutions. Also, the vertical displacements of the static load truck test from a real bridge were well reproduced, taking into account the concrete deck variation. The nodal restrictions when applied to the layered shell element are currently imposed on its middle plane, and then care should be taken on this situation. The response under torsional loads needs further investigation.

In relation to the application of the construction stage analysis of a bridge structure with a box section, the model was able to yield appropriate results for the various scenarios of loading and construction phases, even involving complex sequences of pre-stressing. The obtained displacement and stress histories are similar to those obtained using one-dimensional beam elements. An important fact is that the present modeling technique may allow capturing a realistic biaxial stress field for the concrete deck with loading. This is advantageous as such realistic stresses may indicate potential zones of damage, like cracking.

References

ABAQUS. (2012). *Analysis user's manual version 6.12*. Johnston, RI: Dassault Systemes Simulia Corp.

ACI Committee 209. (1992). *Prediction of creep, shrinkage and temperature effects in concrete structures*. Farmington Hills, MI: American Concrete Institute.

ANSYS. (2007). *Engineering Analysis System Theoretical Manual (Version 11)*. Retrieved from http://www.Ansys.com

Ates, S. (2011). Numerical modelling of continuous concrete box girder bridges considering construction stages. *Applied Mathematical Modelling*, *35*(8), 3809-3820.DOI: https://doi.org/10.1016/j.apm.2011.02.016

Butler, L. J., Lin, W., Xu, J., Gibbons, N., Elshafie, M. Z. E. B., & Middleton, C. R. (2018). Monitoring, modeling, and assessment of a self-sensing railway bridge during construction. *Journal of Bridge Engineering*, *23*(10), 04018076. DOI: https://doi.org/10.1061/(ASCE)BE.1943-5592.0001288

DIANA. (2015). *User's manual version 10.0*. Retrieved from https://manuals.dianafea.com/d100/Diana.html

Dias, M. M., Tamayo, J. L. P., Morsch, I. B., & Awruch, A. M. (2015). Time dependent finite element analysis of steel-concrete composite beams considering partial interaction. *Computers and Concrete*, *15*(4), 687-707. DOI: https://doi.org/10.12989/cac.2015.15.4.687

Haido, J. H., Abu Bakar, B. H., & Abdul-Razzak, A. A. (2010). Dynamic response simulation for reinforced concrete slabs. *Simulation Modelling Practice and Theory*, *18*(6), 696-711. DOI: https://doi.org/10.1016/j.simpat.2010.01.011

Han, C., Zhang, J., Zhou, D., Lan, S., & Wang, P. (2020). Computing creep secondary internal forces in continuous steel-concrete composite beam constructed through segmented pouring. *Journal of Structural Engineering*, *146*(3). DOI: https://doi.org/10.1061/(ASCE)ST.1943-541X.0002494

He, J., Li, X., Li, C., Correia, J. A. F. O., Xin, H., & Zhou, M. (2020). A novel asynchronous-pouring-construction technology for prestressed concrete box girder bridges with corrugated steel webs. *Structures*, *27*, 1940-1950. DOI: https://doi.org/10.1016/j.istruc.2020.07.077

Huang, E., Ke, H., & Hu, H. (2023). Optimization of construction process and determination of intermediate cable forces for composite beam cable-stayed bridge. *Applied Science*, *13*(9), 5738. DOI: https://doi.org/10.3390/app13095738

LARSA. (2021). *Larsa 4d Staged Construction Analysis*. Melville, NY: LARSA, Inc. Retrieved from https://www.larsa4d.com/solutions/staged-analysis.aspx

Li, H., Huang, Y., & Guo, E. (2021).Construction stage vulnerability evaluation of a continuous girder bridge with the cast-in-place cantilever construction method. *Advances in Civil Engineering*, *2021*,9915947. DOI: https://doi.org/10.1155/2021/9915947

Manso, A. N., Martinez, M. A., Diaz, J. J. C., Fresno, D. C., & Rabanal, F. A. (2015). A new steel bridge launching system and method. Fundamentals. *Hormigón y Acero*, *66*(276), 151-163. DOI: https://doi.org/10.1016/j.hya.2015.09.001

MIDAS. (2017). *MIDAS civil on-line manual 2017*. Retrieved from http://manual.midasuser.com/EN_Common/Gen/855/index.htm

Miranda, M. P., Tamayo, J. P., & Morsch, I. B. (2022). Benchmark examples for structural system changes: Analytical and numerical approaches. *Archives of Computational Methods in Engineering*, *29*(6), 3609-3637. DOI: https://doi.org/10.1007/s11831-022-09709-8

Motlagh, H. R. E., & Rahai, A. (2021). Long-term behaviour of a prestressed concrete bridge with corrugated steel webs. *Journal of Bridge Engineering*, *27*. DOI: https://doi.org/10.1061/(ASCE)BE.1943-5592.0001801

Nimse, P. S., Nims, D. K., Hunt, V. J., & Helmicki, A. J. (2015). Use of construction stages to review a Bridge finite-element model. *Journal of Bridge Engineering*, *20*(8), B4015002. DOI: https://doi.org/10.1061/(ASCE)BE.1943-5592.0000731

SAP2000. (2008). *Integrated finite element analysis and design of structures*. Berkeley, CA: Computers and Structures Inc.

Shushkewich, K. W. (1986). Time-dependent analysis of segmental bridges. *Computers and Structures*, *23*, 95-118. DOI: https://doi.org/10.1016/0045-7949(86)90111-2

Su, D., Nassif, H., & Xia, Y. (2018). Optimization of deck construction staging for multiple-span continuous steel girder bridge. *Journal of Performance of Constructed Facilities*, *32*, DOI: https://doi.org/10.1061/(ASCE)CF.1943-5509.0001073

Tadros, M. K., Ghali, A., & Dilger, W. H. (1979).Long-term stresses and deformation of segmental bridges. *PCI Journal*, *24*(4), 66-87. DOI: https://doi.org/10.15554/pcij.07011979.66.87

Tamayo, J. L. P., Morsch, I. B., & Awruch, A. M. (2013). Static and dynamic analysis of reinforced concrete shells. *Latin American Journal of Solids and Structures*, *10*(6), 1109-1134. DOI: https://doi.org/10.1590/S1679-78252013000600003

Vookunnaya, S. S., Ravindranatha, & Thite, T. (2017).Construction stage analysis of segmental cantilever bridge. *International Journal of Civil Engineering and Technology*, *8*(2), 373-382.

Wang, G. M., Zhu, L., Zhou, G. P., Han, B., & Ji, W. Y. (2020). Experimental research of the time-dependent effects of steel–concrete composite girder bridges during construction and operation periods. *Materials (Basel)*, *13*(9), 2123. DOI: https://doi.org/10.3390/ma13092123

Wang, X., Wang, H., Sun, Y., Mao, X., & Tang, S. (2020). Process-independent construction stage analysis of self-anchored suspension bridges. *Automation in Construction*, *117*, 103227. DOI: https://doi.org/10.1016/j.autcon.2020.103227

Wang, Y., Thrall, A., Zoli, T., & Sun, S. (2022). Measuring behaviour of long-span bridges during erection: Case study of the Governor Mario M. Cuomo Bridge. *Journal of Bridge Engineering*, *27*(12), 05022009. DOI: https://doi.org/10.1061/(ASCE)BE.1943-5592.0001954

Zhu, L., Wang, Y., Zhou, G., & Han, B. (2022). Structural health monitoring on a steel-concrete composite continuous bridge during construction and vehicle load tests. *Mechanics of Advanced Materials and Structures*, *29*(10), 1370-1385. DOI: https://doi.org/10.1080/15376494.2020.1820117